11-6-2015

Stochastic models for plant microtubule self-organization and structure

Ezgi Can Eren

Ram Dixit
Washington University in St Louis, ramdixit@WUSTL.EDU

Natarajan Gautam

Noname manuscript No.
(will be inserted by the editor)

Stochastic Models for Plant Microtubule Self-Organization and Structure

Ezgi C. Eren · Ram Dixit · Natarajan Gautam

Received: date / Accepted: date

Abstract One of the key enablers of shape and growth in plant cells is the cortical microtubule (CMT) system, which is a polymer array that forms an appropriately-structured scaffolding in each cell. Plant biologists have shown that stochastic dynamics and simple rules of interactions between CMTs can lead to a coaligned CMT array structure. However, the mechanisms and conditions that cause CMT arrays to become organized are not well understood. It is prohibitively time-consuming to use actual plants to study the effect of various genetic mutations and environmental conditions on CMT self-organization. In fact, even computer simulations with multiple replications are not fast enough due to the spatio-temporal complexity of the system. To redress this shortcoming, we develop analytical models and methods for expeditiously computing CMT system metrics that are related to self-organization and array structure. In particular, we formulate a mean-field model to derive sufficient conditions for the organization to occur. We show that growth-prone dynamics itself is sufficient to lead to organization in presence of interactions in the system. In addition, for such systems, we develop predictive methods for estimation of system metrics such as expected average length and number of CMTs over time, using a stochastic fluid-flow model, transient analysis, and approximation algorithms tailored to our problem. We illustrate the effectiveness of our approach through numerical test instances and discuss biological insights.

Ezgi C. Eren
PROS, Inc., 3100 Main Street, Suite #900, Houston, TX 77002, USA
E-mail: eeren@pros.com

Ram Dixit
Department of Biology, Washington University in St. Louis, Campus Box 1137, St. Louis, MO 63130-1137, USA
E-mail: ramdixit@biology2.wustl.edu

Natarajan Gautam
Department of Industrial and Systems Engineering, Texas A&M University, Mailstop 3131, College Station, TX 77843-3131, USA
E-mail: gautam@tamu.edu

Keywords stochastic fluid-flow models · mean-field theory · simulation · spatio-temporal bio-processes · plant cell cortical microtubules

1 Introduction

The cortical microtubule (CMT) cytoskeleton of plant cells (see Figure 1) is essential for development of cell shape, maintenance of cell structure, and other critical functions including directional transport of cellular material. CMTs are polymers of tubulin subunits that are organized into distinctive arrays according to the cell type and function. They reside on an approximately planar area, as they are attached to the cell surface (cortex) (Barton et al, 2008; Hardham and Gunning, 1978). As a result of their dynamic behavior on the cortex, CMTs encounter each other which result in interactions that change their orientation or their dynamic state (Dixit and Cyr, 2004a). Starting as disorganized CMTs that are distributed randomly over the cortex and growing in random directions, CMTs are observed to self-organize into a coaligned pattern over time (Dixit and Cyr, 2004b; Ehrhardt and Shaw, 2006; Wasteneys and Ambrose, 2009). Our objective is to develop methods to model and analyze the self-organization in this system as well as other key measures that define the CMT array structure such as average CMT length and number.

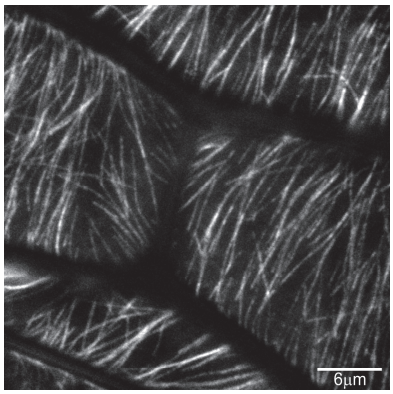

Fig. 1 Cortical microtubules in epidermal cells of the hypocotyl (i.e., embryonic stem) of an Arabidopsis plant expressing green fluorescent protein-labeled tubulin.

CMT organization is achieved despite the lack of any central control mechanism, relying primarily on the individual *dynamics* of CMTs and *interactions* among them. Exploring mechanisms that drive CMT organization is crucial, as the degree of aligned CMT organization and array structure are critical determinants of cell shape. This motivates the question of whether it would be possible to replicate this self-organization by simulating CMT dynamics and interactions. For this, we previously developed a computer simulation model

(Eren et al, 2010) that replicates CMT dynamics and interactions based on the data from biological experiments (microscopy studies of live plant cells) in rapidly elongating wild-type cells (Shaw et al, 2003) and two different mutants (Burk and Ye, 2002; Burk et al, 2001; Kawamura and Wasteneys, 2008). This study revealed that an initially disorganized set of CMTs can indeed self-organize into ordered arrays as seen in the snapshots of the system at different time points of the simulated example in Figure 2 (also reported in Allard et al (2010), Tindemans et al (2010) and Deinum et al (2011)). Simulating with different parameter sets from wild-type cells and mutants as well as self-generated data, the impacts of different mechanisms on organization were identified, some of which we will refer to while building the models presented in this paper as well as discussing results.

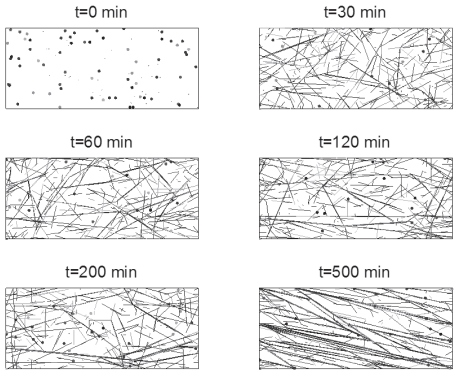

Fig. 2 Snapshots of the Simulated CMT System at Different Time Points (Parameter Set I in Appendix 1)

Despite providing a means to model the CMT system by mimicking its spatio-temporal complexity as close as possible to that in cells, simulations are nonetheless computationally expensive to conduct enough replications to yield generalized conclusions. This is more emphasized for the settings with growth-prone dynamics as seen in wild-type cells (Kawamura and Wasteneys, 2008; Shaw et al, 2003) due to the system getting too crowded relatively early in the course of the simulations. Hence, in this paper, we formulate analytical techniques that are more efficient and lead to more generalized results and conclusions based on our conjectures from the simulations. We develop a fluid model to theoretically determine a region of system parameters that guarantee CMT organization. Subsequently, focusing on that region, we develop predictive methodologies for other measures that characterize the CMT array structure such as average length and number, which -to the best of our knowledge- have not been analytically studied earlier.

Several groups have developed quantitative models with varying assumptions to study CMT organization, which show that CMT dynamics and interactions can produce ordered arrays as observed in plant cells under different conditions (Allard et al, 2010; Baulin et al, 2007; Dixit and Cyr, 2004a; Hawkins et al, 2010; Shi and Ma, 2010; Tindemans et al, 2010). In addition to computer simulations, there are various analytical techniques that have been used to model CMT systems and their organization. Baulin et al (2007) formulated diffusion equations that represent CMT dynamics and interactions, and approximated the impact of interactions based on the kinetic theory of gases. Hawkins et al (2010) built a continuum model where different types of CMT interactions were considered and conducted a bifurcation study around the isotropic (disorganized) solution to investigate parameter regions where organization is possible. Shi and Ma (2010) conducted a similar bifurcation analysis for their model, in which they formulated interactions using mean-field theory. A more detailed review of the methodologies and results of these previous studies can be found in Eren et al (2012).

The results from previous studies differed in terms of the impact of different mechanisms on CMT organization, probably because of differences in microtubule dynamicity parameters and the assumptions for interaction mechanisms between these studies (Eren et al, 2012). Here, we define two regimes called 'bounded growth' and 'unbounded growth' based on the state transition parameters of single CMT dynamics similar to Dogterom and Leibler (1993). Hawkins et al (2010) and Tindemans et al (2010) consider parameters that fall under 'bounded growth' regime only and the possibility of organized solutions for that region. Dynamicity parameters used in simulations of Allard et al (2010) include data sets that fall under both regimes, however the mean length seems to stay finite in all their simulations suggesting existence of another parameter that bounds microtubule length explicitly. Baulin et al (2007) study a relatively simplistic setting with no state transitions, which is a limiting case of 'unbounded growth' with deterministic movements at both ends. Shi and Ma (2010) seems to be the only study to consider the impact of dynamicity parameters in both regions, however keeping growth bounded by an explicit upper bound on maximum length that can be reached by any CMT. Our paper brings a different approach where we do not explicitly limit CMT length mainly as the major limiting factors on CMT growth have not been measured yet. Our choice of growth-prone dynamics is supported by experimental data from independent studies (Ishida et al, 2007; Kawamura and Wasteneys, 2008; Shaw et al, 2003; Vos et al, 2004; Zhang et al, 2013), some of which we use to build the data sets used in our study. Our analysis reveals that a quasi-steady-state can still be reached due to the CMT interactions, which points to an intrinsic mechanism to keep growth limited for a finite amount of time as organization settles. In addition, we explicitly consider the stochastic nature of CMT dynamics and interactions, and use a variety of analytical techniques to model and develop descriptive and predictive methods for different CMT array characteristics.

This paper is organized as follows. In Section 2, we describe the system, introduce the modeling details and the mathematical framework for our models. In Section 3 we describe the mean-field model for system organization together with its analysis and results. In Section 4, we present the fluid model for single CMT dynamics and related methods for estimation of system metrics. We refer to simulations as relevant and include a numerical comparison of outputs to simulation results. Finally, we conclude in Section 5 with a discussion of the major insights derived from this study, summary of contributions, and possible extensions and applications of the developed methodologies.

2 System Description, Mathematical Notation and Framework

We begin by describing the CMT system in detail and constructing a mathematical notation and framework employed in the rest of the paper (Section 2.1). We mostly include details relevant to the modeling approach and refer the reader to Eren et al (2010) for an explanation of the system with further biological details. Following this, we introduce the quantification metrics used for characterization of system properties and organization (Section 2.2).

2.1 CMT System, Modeling Details and Notation

Our description and modeling of the CMT system are based on experimental evidence from relevant literature (Dixit and Cyr, 2004a; Shaw et al, 2003). CMTs are filamentous structures that have an approximately linear shape. They are formed by head-to-tail assembly of tubulin dimers which are the building blocks (see Figure 3). One end of the CMTs is highly dynamic and "grows" on average, which is designated as the "leading end"; whereas the other end is less dynamic, "shortening" on average and accordingly called the "lagging end". More specifically, the leading end stochastically switches between *growth* (G), *shortening* (S) and *pause* (P) phases, whereas the lagging end alternates only between *shortening* (S) and *pause* (P) phases. Growth occurs by the addition of tubulin subunits to the leading end, and shortening occurs by loss of tubulin subunits from either end.

We indicate CMTs by $i = 1, ..., I(t)$, where $I(t)$ is the total number of CMTs in the system at time t. Note that a CMT can have more than one segment as a result of bundling with other CMTs. Let $N_i(t)$ be the number of segments of CMT i at time t, for all $i = 1, 2, ..., I(t)$. We denote the orientation and length of n^{th} segment of the i^{th} CMT at time t by $\theta_i^n(t)$ and $l_i^n(t)$ respectively, where $\theta_i^n(t) \in \Phi^{360} = \{0^0, 1^0, ..., 359^0\}$ (see Figure 4 for a representative sketch). Note that the segments of CMTs are counted according to the order they appear. Hence, the leading end of CMT i is located at its $N_i(t)^{th}$ segment at time t, whereas the lagging end is always at the first segment. The total length for CMT i at time t is given by $L_i(t) = \sum_{n=1}^{N_i(t)} l_i^n(t)$. Note that a CMT i disappears and departs the system if it shrinks to length zero. The

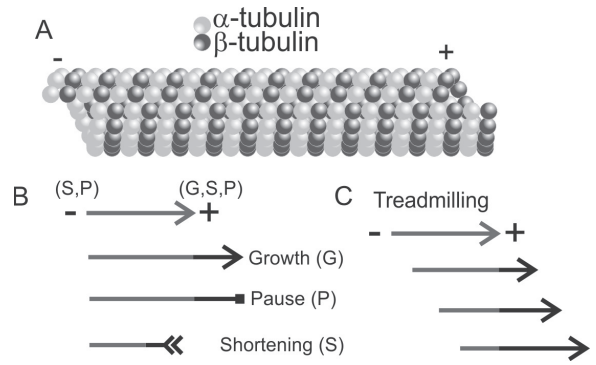

Fig. 3 A. CMT Tubulin Structure with Leading (+) and Lagging (-) Ends. B. Leading end dynamics consist of Growth, Pause and Shortening phases. C. CMTs show treadmilling dynamics due to net growth at the leading end and net shortening from the lagging end.

indices are renumbered accordingly every time a CMT departs or a segment disappears due to shortening of the lagging end. Dynamics of CMT i are

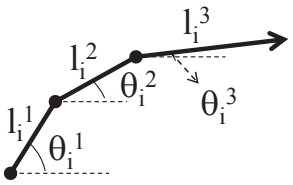

Fig. 4 Sketch of a CMT with Multiple Segments and the Corresponding Variables

governed by independent and identical environment process $\{M_i(t) : t \geq 0\}$ corresponding to its state which is defined as a combination of leading and lagging end phases. The environment process is modeled as a continuous-time Markov chain (CTMC) with an infinitesimal generator matrix $Q = [q_{m,n}]$, $m, n \in \{GS, GP, SS, SP, PS, PP\}$, by assuming that both ends spend an exponentially distributed amount of time in each phase and switch to one of the other possible phases, similar to the assumption in Allard et al (2010). A sample path for the state of a CMT with the corresponding length graph is plotted in Figure 5. Note that while in a growth or shortening state, the length of the CMT changes with a constant velocity during the sojourn in that state. The absolute speeds corresponding to each phase are given by the matrix $v^+ = diag(v_{G^+}, v_{S^+}, v_{P^+})$ for the leading end, and by the matrix $v^- = diag(v_{S^-}, v_{P^-})$ for the lagging end. Note that $v_{P^+} = v_{P^-} = 0$, since the speed is zero in the pause phase. As a result, we can define a diagonal net speed matrix $V = diag(v^m) = diag(v_{G^+} - v_{S^-}, v_{G^+}, -v_{S^+} - v_{S^-}, -v_{S^+}, -v_{S^-}, 0)$ that composes of the net speeds for each state $m \in \{GS, GP, SS, SP, PS, PP\}$, generated according to Q.

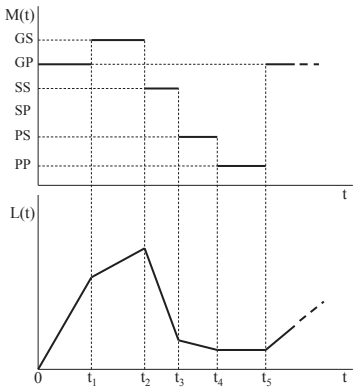

Fig. 5 Realization of the Length Process, $L(t)$ of a CMT Based on its State, $M(t)$

CMTs appear randomly over time from multiple locations that are dispersed throughout the cell cortex. The orientation of CMTs is determined by the growth direction of their leading ends. As a result of the distinct dynamics at both ends, a CMT moves in the direction that its leading end grows (Shaw et al, 2003). Because CMTs are attached to the plasma membrane surface, they run into other CMTs in the system, which results in CMT interactions. These interactions occur on an approximately planar area and can affect the dynamics and orientation of the CMT as illustrated in Figure 6. It is possible to state some basic rules to explain the CMT interactions based on the experimental data (Dixit and Cyr, 2004a). The outcome of any interaction depends on the collision angle, α, and a critical interaction angle specific to the system, θ^c. If a CMT runs into another one (that we call the barrier) with a collision angle that is less than the critical interaction angle, i.e. $\alpha \leq \theta^c$ (see Figure 6), with probability p_b, its leading end bends in the direction of the barrier and continues to grow along it forming a bundle at the point of collision. This "bundling" would happen with some curvature, however we are approximating it by a linear shape in the figure and accordingly modeling it as generation of an additional segment with a parallel orientation to that of the barrier. As a result, the leading end is located at the tip of the new segment, whereas the lagging end stays at its original location on the already existing segment. If the collision angle is greater than the critical interaction angle, i.e. $\alpha > \theta^c$, the CMT undergoes catastrophe, which means that its leading end immediately leaves the growth phase and transitions into the shortening phase, with probability p_c. The third possible outcome is that the CMT crosses over the barrier neither changing its orientation nor state, which happens with probability $(1 - p_b)$ for the $\alpha \leq \theta^c$ case and with probability $(1 - p_c)$ for the $\alpha > \theta^c$ case.

In summary, the matrices Q and V regulate the single CMT dynamics, and the interactions are controlled by θ^c, p_b, and p_c parameters, which are measured experimentally and observed to take on different values depending on

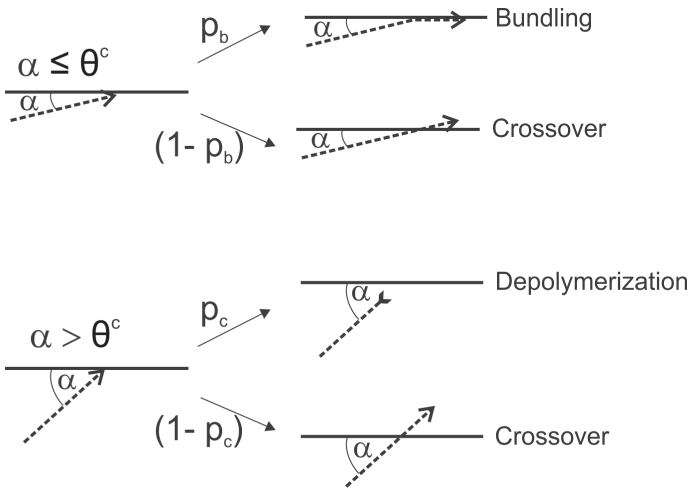

Fig. 6 Outcomes of CMT Interactions. A preexisting barrier CMT is shown as a solid line, while a new CMT is shown as a dashed line with the arrow head indicating its leading end. At contact angles less than theta, CMTs either reorient their leading end and grow along the barrier CMT (with probability p_b), or cross over the barrier CMT. In contrast, at contact angles more than theta, CMTs switch to depolymerization (with probability p_c) or cross over the barrier CMT.

plant cell type, genetic background and environmental conditions as reported by independent studies (Burk and Ye, 2002; Burk et al, 2001; Kawamura and Wasteneys, 2008; Shaw et al, 2003), which we use as data sets (listed in Appendix 1) for our study.

Additionally, new CMTs are introduced into the system following a Poisson process with an appearance rate of λ_a at a location uniformly distributed across the cell surface. The initial length of any CMT, l_0, is typically tiny and the initial angle (orientation) assigned to it belongs to the set Φ^{360}. Initially there are $I(0)$ CMTs in the system with a length of l_0, and orientation for each CMT sampled from a discrete uniform distribution. The complete set of input parameters including the ones for the initial conditions of the system is given in Table 1.

2.2 Metrics for Quantification of System Organization and Structural Properties

In order to analyze conditions that lead to CMT organization, we need a method to quantitatively measure the level of organization in the system. To characterize the degree of coalignment in a given CMT array, we first describe angular distributions of CMTs weighted with respect to their length. We classify CMT segments according to their orientation, so that each segment belongs to one of the classes $\theta' \in \Phi^{180} = \{0, ..., 179\}$. For this, each segment with $\theta_i^n(t)$ in $\{0^0, ..., 179^0\}$ is assigned to the same class as its angle, whereas

Table 1 Input Parameters

Notation	Parameter
Dynamicity Parameters	
$Q = [q_{m,n}]$	infinitesimal generator for the state process
$V = diag(v^m)$	velocity matrix for the CMT states
Interaction Parameters	
θ^c	critical interaction angle
p_b	bundling probability
p_c	catastrophe probability
Parameters Related to the Arrival Process and Initial Conditions	
λ_a	appearance rate for new CMTs
l_0	initial length of an appearing CMT
$I(0)$	initial number of CMTs in the system

each segment with $\theta_i^n(t)$ in $\{180^0, ..., 359^0\}$ is mapped to class $\theta_i^n(t) - 180$. In other words, we distinguish CMT segments by their slopes rather than their exact orientations, as their alignment is the actual determinant of the organization level. For each $\theta' \in \Phi^{180}$, we calculate

$$k(\theta', t) = \frac{\sum_{i=1}^{I(t)} \sum_{n=1}^{N_i(t)} l_i^n(t) 1_{\{\theta_i^n(t) \to \theta'\}}}{\sum_{i=1}^{I(t)} \sum_{n=1}^{N_i(t)} l_i^n(t)}, \tag{1}$$

where $1_{\{\theta_i^n(t) \to \theta'\}}$ stands for the indicator function of whether the angle $\theta_i^n(t)$ belongs to class θ'. Note that Equation (1) represents the ratio of the total length of segments which belong to class θ' to the total length of all CMT segments in the system at time t.

In order to characterize the angular distribution of CMTs, we employ Shannon's entropy formula (Martin et al, 2006; Shannon, 1948), which quantifies the diversity or uniformity level of a system for any property of interest and is widely used in the literature as a measure of the uncertainty in a random variable and to quantify organization (Gray, 1990; Lu et al, 2008). Applying the entropy metric on the angle distributions of CMTs given by Equation (1), entropy of the system at time t, $H(t)$, is given by

$$H(t) = -\sum_{\theta'=0}^{179} k(\theta', t) ln\left(k(\theta', t)\right). \tag{2}$$

Equation (2) would approach its maximum value of $-\ln(1/180) = 5.19$ if CMTs were perfectly uniformly distributed with respect to their alignment and a minimum value of 0 if all CMTs had the same alignment. Simulations that lead to organized CMT systems starting with a disorganized array show decreasing entropy (after a small transient increase early in the simulations), as CMTs continuously transform into better ordered arrays over the course of the experiment (See Figure 7(i) for sample entropy plots of ten independent simulation runs with the same data set).

Some other metrics that are essential to characterize the CMT array are the total number of CMTs in the system and the average CMT length over

time. Even for a perfectly organized system only based on angular alignment, the CMT array can still be defective if there is not an ideal structure in terms of the array density as well (some examples of perfectly organized defective CMT arrays would be a few very long perfectly aligned CMTs, or a bunch of very short perfectly aligned CMTs). For this, we develop methodologies to predict metrics related to CMT density as well as studying CMT organization for a given system. Total number of CMTs present in the system at time t is given by $I(t)$ as described in Section 2.1, and the average CMT length at time t is given by

$$\bar{L}(t) = \frac{\sum_{i=1}^{I(t)} \sum_{n=1}^{N_i(t)} l_i^n(t)}{I(t)}. \tag{3}$$

Those two metrics can also be used to define the total CMT length in the system by

$$\sum L(t) = I(t)\bar{L}(t), \tag{4}$$

which also gives a measure of the crowdedness (or density) of CMTs for a given area.

3 Mean-field Model for Microtubule Organization

3.1 Objectives and Relation to the Simulation Results

As discussed briefly in Section 1, different system behavior and properties are observed in CMT simulations (as well as in plant cells) for different parameters of dynamicity and interactions. Here, we classify these outputs into three distinct categories. Before introducing this classification of the system structure, we introduce the related terminology that we use in Definitions 1 and 2.

Definition 1 A CMT system is defined as disorganized if the entropy metric given by Equation (2) satisfies $H(\infty) = 5.19$; and it is defined as ideally organized if $H(\infty) = 0$.

Note that one does not observe ideally organized conditions in plant cells and simulations but a dominant angle (or range of angles) emerges that we informally define as "organized" and $H(\infty)$ is significantly smaller than 5.19.

Definition 2 A deterministic system metric $G(t)$ (particularly, $I(t)$ or $\bar{L}(t)$) is defined to be stable if $G(\infty) < \infty$; and it is defined to be unstable otherwise, i.e. $G(\infty) = \infty$.

We use the term *quasi-stable* for the metrics that are unstable in the long-run, however are able to stabilize temporarily for a finite amount of time.

Our classification of possible system behavior based on simulation results is as follows:

1. *Organized, quasi-stable* case, where angle distributions of CMTs are biased towards a dominant angle in time and accordingly entropy values are continuously decreasing; and system metrics such as average length and number of CMTs temporarily stabilize around a constant value after an initial increase as organization settles. Note that *organized, stable* case is a sub-case of this where the system is able to reach a true steady state and stay there continually rather than a finite amount of time.
2. *Disorganized, stable* case, where CMTs stay disorganized with non-decreasing entropy values and a corresponding angle distribution close to uniform; and system metrics stay finite around a rather low value. In such systems, CMTs do not grow long and crowded enough to interact.
3. *Disorganized, unstable* case, where CMTs stay disorganized and system metrics keep increasing indefinitely. In such systems, CMTs do not interact enough to generate organization despite running into each other.

By stability, we refer to system metrics such as length and number remaining finite over time as in Definition 2. Sample plots of independent simulation results for all three cases are presented in Figure 7. The plots show realizations of average length of CMTs vs. time, however the realizations for number of CMTs vs. time show quite similar characteristics. Corresponding entropy plots that give a measure of organization level in time are also provided.

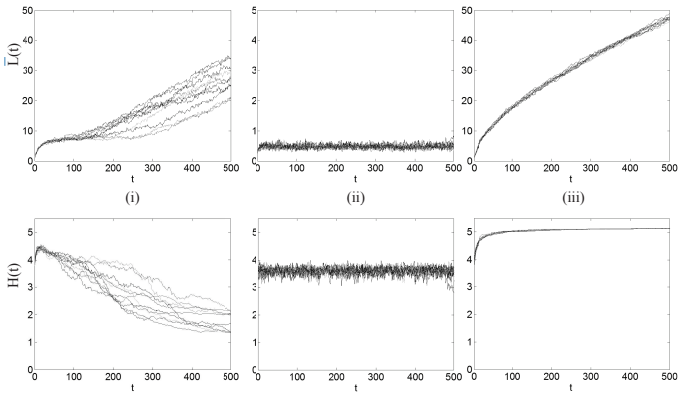

Fig. 7 Sample Average Length and Entropy for Simulations of Cases (i), (ii) and (iii): (i) Parameter Set I; $p_b = 1$, $p_c = 0.3$, $\theta^c = 40^o$; (ii) Parameter Set V; $p_b = 1$, $p_c = 0.3$, $\theta^c = 40^o$; (iii) Parameter Set I; $p_b = 0$, $p_c = 0$, $\theta^c = 40^o$

Among the three, case (i) is what is observed in wild-type plant cells where CMTs exist as organized arrays according to data from biological experiments (Eren et al, 2010). This organization may be perturbed by genetic mutations or environmental conditions (as discussed in Section 1) that cause a change in system parameters, which results in one of the other cases. We are particularly interested in exploring conditions for case (i) to be guaranteed, which would

facilitate engineering of settings that will maintain or generate particular organization in plant cells.

3.2 Model Equations and Analysis

3.2.1 Problem Formulation

We consider a mean-field model where CMTs are distributed homogeneously on a two-dimensional surface. We alter the bundling mechanism for modeling purposes as follows: In the case of a bundling event, the colliding CMT of length l completely aligns with the barrier CMT with probability $p_b(l)$ rather than forming a new segment. That is, with a certain probability which is a function of length, the CMT changes its orientation parallel to that of the barrier. This assumption can be explained in terms of two possibilities after a bundling event: Either the newly formed segment would shrink to zero length as a result of leading end dynamics or the former segment(s) would disappear as a result of shortening at the lagging end. Both of these events define stopping times (let us call them τ_1 and τ_2 in relative order); and $p_b(l)$ can be expressed as $P(\tau_1 < \tau_2)$, which is a decreasing function of CMT length before bundling, l. As a result, the bundling probability is considered as a decreasing function of the CMT length to account for the fact that bundling is more likely to be reversible for relatively longer CMTs due to different dynamics at the leading and lagging ends; other than this assumption, it is kept as a general function. This mechanism allows us to model each CMT as a single segment throughout its lifetime. It was tested and verified using simulations that this assumption does not change the overall system characteristics defined in Section 2.2. In fact one supporting observation from our simulations is that average number of segments per CMT stays well below 2 throughout the runs with our major parameter sets that we use in this study. Based on these assumptions we derive an integro-differential equation system as follows. We define $p_m(l, \theta, t)$ as the density of CMTs with length l and angle θ that are at state m at time t, where $m \in \{GS, GP, SS, SP, PS, PP\}$. The generic equation can be stated to be of the form:

$$\frac{\partial p_m(l,\theta,t)}{\partial t} = -v^m \frac{\partial p_m(l,\theta,t)}{\partial l} + \sum_n q_{n,m} p_n(l,\theta,t) + J_m(l,\theta,t), \qquad (5)$$

where $J_m(l, \theta, t)$ correspond to the interactions (and the remaining due to the dynamics), $0 < l, t < \infty$ and $\theta \in \Phi^{180} = \{0, 1, ..., 179\}$. Formulation of Equation (5) follows conditioning on state transitions into state m from all states n in a positive small time interval (Δt) and factoring corresponding transition probabilities and length change to get:

$$p_m(l,\theta,t+\Delta t) = p_m(l-v^m\Delta t,\theta,t)(1+q_{m,m}\Delta t) + \sum_{n\neq m} p_n(l-v^n\Delta t,\theta,t) q_{n,m}\Delta t + o(\Delta t), \qquad (6)$$

where $o(\Delta t)$ is a collection of terms of higher order than Δt such that $o(\Delta t)/\Delta t \to 0$ as $\Delta t \to 0$. Subtracting $p_m(l,\theta,t)$ from each side of the equation and dividing by Δt, we obtain the dynamics related terms in Equation (5) by letting $\Delta t \to 0$. The interaction related term, $J_m(l,\theta,t)$ in Equation (5) is formulated using the critical interaction angle θ^c to determine the relative frequencies of bundling/catastophe for each angular value. $p_b(l)$ and p_c are used as coefficients for loss/gain of density as a result of bundling and catastrophe relatively, where the frequency of interactions are approximated as a function of sine of the difference in angles of the two colliding CMTs similar to the methodology in Hawkins et al (2010). Based on this, the formulation for state $m = GS$ is given by

$$\begin{aligned} J_{GS}(l,\theta,t) = &- v_G^+ p_{GS}(l,\theta,t)\Big[\sum_{\theta'\in\Theta} p_c|sin(\theta-\theta')|\int_{l'} dl'l'\bar{p}(l',\theta',t) \\ &+ \sum_{\theta'\in\Theta^*} p_b(l)|sin(\theta-\theta')|\int_{l'} dl'l'\bar{p}(l',\theta',t)\Big] \\ &+ \Big(\int dl'l'\bar{p}(l',\theta,t)\Big)\sum_{\theta'\in\Theta^*} v_G^+ p_{GS}(l,\theta',t)p_b(l)|sin(\theta-\theta') \end{aligned} \tag{7}$$

where

$$\Theta = \{\theta+\theta^c+1,...,\theta+(180-\theta^c)-1\} \ \ mod \ \ 180 \ \ ,$$
$$\Theta^* = \{0,1,...,179\} - \Theta - \{\theta\} \ \ mod \ \ 180,$$

where the "mod" function is to adjust all the negative degrees and degrees that are equal to or greater than 180 in Θ and Θ^* to fall in the set Φ^{180}; and $\bar{p}(l,\theta,t)$ denotes the total density of CMTs with length l and angle θ at time t. The first term represented in the first two lines of Equation (7) stands for the density loss due to CMTs in state GS with length l and angle θ running into other CMTs and bundling with them or undergoing catastrophe. Since bundling changes the angular orientation of a growing CMT, it results in a density loss in the starting orientation (i.e., orientation prior to bundling), and also a density gain in the new CMT orientation (i.e., orientation after bundling). Hence, Equation (7) contains another term in the last line related to bundling to represent the density gain from CMTs that are in state GS with length l running into a CMT with angle θ and switching their orientation to θ by bundling with it. The interaction frequencies are functions of the growth speed of the leading end rather than the net speeds of growing CMTs, as collisions are directly generated by the dynamics of the leading end.

Finally, the boundary condition is given as a function of the appearance rate:

$$p_{GS}(0,\theta,t) = \frac{\lambda_a}{180A}, \tag{8}$$

were A is the area of the surface that CMTs reside on. The boundary condition indicates that CMTs appear with a 0 length in the GS state without loss of generality. Equation (8) is just presented for the sake of completeness and does not affect the analysis and results in the following sections.

3.2.2 Equilibria Analysis

Having derived an integro-differential equation system for the dynamics and interactions of CMTs, we begin by searching for equilibrium points and use Lyapunov stability concepts to characterize them (Khalil, 2002; Long et al, 2008). By stability, here we imply the convergence of solutions in time towards an equilibrium point rather than the stability notion used to characterize system properties in Section 3.1. Reaching an equilibrium point does not guarantee stability, and recall that we denote this condition quasi-stability. An equilibrium point of (5) given by $\frac{\delta p_m(l,\theta,t)}{\delta t} = 0$ for all $m \in \{GS, GP, SS, SP, PS, PP\}$ is

$$P^* = \{(p_{GS}(l,\theta,t),\ p_{GP}(l,\theta,t),\ p_{SS}(l,\theta,t),\ p_{SP}(l,\theta,t),\ p_{PS}(l,\theta,t),\ p_{PP}(l,\theta,t)) \\ s.t.\quad k(\theta^*,t) = 1,\ k(\theta,t) = 0\ \ \forall \theta \neq \theta^*\}, \tag{9}$$

where $k(\theta,t)$ is given by Equation (1) in Section 2. Note that Equation (9) corresponds to an ideally organized solution where all CMTs in the system are aligned with the same orientation. We employ the entropy metric defined in Equation (2) as a Lyapunov function to establish conditions for stability. Use of entropy as a Lyapunov function is rarely seen in the related stability literature. Here, its use is intuitive as organization is directly characterized by entropy and the function meets Lyapunov criteria for the given equilibrium point as follows. We reformulate the angle distribution used in Equation (2) in line with the notation from the mean-field model as follows:

$$\forall \theta, t, \qquad k(\theta,t) = \frac{\int_0^\infty l\bar{p}(l,\theta,t)dl}{\sum_{\theta=0}^{179}\int_0^\infty l\bar{p}(l,\theta,t)dl}, \tag{10}$$

For the solution given by Equation (9), since $k(\theta^*,t) = 1$ and $k(\theta,t) = 0\ \forall\ \theta \neq \theta^*$, the entropy of the system is zero, which we will denote by $H(t)\ |_{P=P^*} = 0$. For all other solutions $P \neq P^*$, the entropy is positive, i.e. $H(t)\ |_P > 0$. Hence, Equation (2) can be used as a Lyapunov function for characterizing the equilibrium point P^*. Prior to stating our main result of this section in Proposition 1, we provide a lemma which is used in its proof.

Lemma 1 *Given two different sequences* $(x_1, x_2, ...x_N)$ *and* $(y_1, y_2, ...y_N)$ *with* $x_i > 0$, $i = 1, ..., N$ *and* $\sum_{i=1}^N x_i = 1$, $\sum_{i=1}^N y_i = 1$*; assume that for any two pairs of* x_i, y_i *and* x_j, y_j, $i, j = 1, ..., N$, $x_i \geq x_j$ *if and only if* $y_i \geq y_j$ *and* $(y_i - x_i) \geq (y_j - x_j)$*, i.e. sequences and their difference increase and decrease in the same order. Let* $f(x) > 0$ *be a decreasing function of* x*. Then the following inequality holds*

$$\sum_{i=1}^{N} f(x_i)(y_i - x_i) < 0. \tag{11}$$

Proof: See Appendix 2. □

Proposition 1 *For a system with $p_b(l), p_c > 0$, a sufficient condition for the global asymptotic stability of P^* defined in (9) is given by*

$$p_G^+(t)v_{G^+} - p_S^+(t)v_{S^+} - p_S^-(t)v_{S^-} > 0,$$

where $p_G^+(t)$ and $p_S^+(t)$ stand for the total density of CMTs that have a growing and shortening leading end in respective order at time t. Similarly, $p_S^-(t)$ stands for the total density of CMTs that have a shortening lagging end at time t. In other words,

$$p_G^+(t) := \sum_\theta \int_0^\infty (p_{GS}(l,\theta,t) + p_{GP}(l,\theta,t))dl,$$

$$p_S^+(t) := \sum_\theta \int_0^\infty (p_{SS}(l,\theta,t) + p_{SP}(l,\theta,t))dl,$$

$$p_S^-(t) := \sum_\theta \int_0^\infty (p_{GS}(l,\theta,t) + p_{SS}(l,\theta,t) + p_{PS}(l,\theta,t))dl.$$

Proof: See Appendix 2. □

The inequality in the proposition ensures a positive net change in CMT length on average. We conjecture that this condition will be satisfied if

$$\pi V := \pi_G^+ v_G^+ - \pi_S^+ v_S^+ - \pi_S^- v_S^- > 0, \tag{12}$$

where π_G^+ and π_S^+ stand for the long-run probabilities that the leading end is in growth and shortening phases in respective order; and π_S^- is the long-run probability that the lagging end is in shortening phase. These long-run probabilities are derived using infinitesimal generator Q and $\pi Q = 0$, where $\pi = [\pi_{GS}\ \ \pi_{GP}\ \ \pi_{SS}\ \ \pi_{SP}\ \ \pi_{PS}\ \ \pi_{PP}]$ holds the long-run probabilities of CMT dynamic states, and $\pi_G^+ = \pi_{GS}+\pi_{GP}$, $\pi_S^+ = \pi_{SS}+\pi_{SP}$, $\pi_S^- = \pi_{GS}+\pi_{SS}+\pi_{PS}$.

πV stands for the net average length change for a single CMT ignoring interactions in the system. Hence, having it positive as implied in Equation (12) corresponds to *growth-prone* dynamics that we defined in Section 1. The system reaches a quasi-stable state as a result of interactions increasing the transition from growth to shortening phase which is captured in the interaction-related terms of Equation (5). Indeed, it is impossible to reach a true steady state in the long run as the length grows unboundedly with organization settling and interaction frequencies no longer limiting growth. Unbounded growth is an artifact of simulation and analytical models as normally in plant cells growth would be bounded by the limited tubulin amount in the system. However, as described in Section 1, we ignore this limit as it is not measured in biological experiments so far. The unlimited growth seen after organization does not impact the results of our study as we are interested in the time frame until the end of quasi-stabilization phase. Note that the time to reach the quasi-stabilization phase matches the time it takes for CMTs to organize in plant cell experiments (Dixit et al, 2006; Eren et al, 2010).

Table 2 πV Values for Different Parameter Sets

Parameter Set	Status	πV
I	organized	0.260
II	organized	0.017
III	organized	1.733
IV	organized	-0.106
V	disorganized	-0.763
VI	organized	0.963

Proposition 1 and our related conjecture show that CMT organization is roughly robust to interaction parameters as long as CMTs are growing on average. This outcome is expected since interactions are easily kept at a high frequency regardless of the particular values of p_b and p_c as long as they are not set to zero. In fact, for the case $\sum L'(t) < 0$, following similar procedure as in the proof of Proposition 1, our conjecture is that organization can be achieved especially for values close to zero, but this is heavily dependent on interaction parameters maintaining a certain frequency of bundling and catastrophe.

3.3 Comparison to Simulation Results

Results derived by analysis of the mean-field model are in line with our observations from simulations with different data sets. In order to test them numerically, Table 2 lists the organization results for different parameter sets given in the Appendix 2 according to simulations and the corresponding value of πV for each case. Note that these are all experimentally derived data sets by independent studies, where the behavior seen in real plant cells were successfully replicated using our simulations (Eren et al, 2010). As seen in Table 2, cases I, II, III and VI satisfy the sufficient condition for organization given in Equation (12) and result in organized arrays regardless of the interaction parameters. In contrast, case V fails to produce organized arrays since the dynamicity parameters correspond to an average net velocity that is significantly less than zero. On the other hand, case IV achieves organization despite not satisfying the sufficient condition, but it is heavily dependent on the interaction parameters as discussed in Section 3.2.2. As the condition we derived is a sufficient one but not necessary, it might still be possible to have organization when it is not satisfied, especially for the cases where the average net velocity is close to zero.

4 Fluid Model for Lifetime of a Single Microtubule and Approximation of System Metrics

Having analytically derived a sufficient condition for self-organization of CMTs, we develop methods to estimate the average length and number of CMTs for the parameter region that this condition holds. Among the cases discussed

in Section 3.1, the *organized quasi-stable* case, which meets the derived organization condition in Equation (12), is the most challenging to estimate such metrics, due to its complex and chaotic properties. Increased and time-varying frequency of interactions over the course of organization results in a high variation of metrics between simulation runs as seen in case (i) of Figure 7. For settings that are in the bounded growth region, regardless of their organization state, the system will ultimately reach and persist at a stable state where both the interaction and state transition frequencies stay at their long-run average. For systems that stay disorganized and are in the unbounded growth region (case (iii) in Figure 7), interactions can in general be ignored (in fact, based on our main result of Section 3), such systems can stay disorganized only in the absence of interactions) and the system metrics can be estimated mainly based on single CMT dynamics. However, in organizing systems, interaction frequencies change dynamically according to the status of organization. In order to develop a predictive method that can capture this dynamicity and complexity, we employ a combination of various techniques including a fluid model for single CMT dynamics, simulations and approximation algorithms. We limit the time of estimation until the end of quasi-stabilization due to the reasons explained in Section 3.2.2.

4.1 Model and Analysis for Single CMT Dynamics

As described in Section 2, the total length of CMT i at time t is denoted by $L_i(t)$. In the following, we remove index i from our notations, as we are considering single CMT dynamics. The length of a CMT at time t, $L(t)$, changes according to its state at time t, $M(t)$ (see Figure 5). Accordingly, the dynamics of the length process, $\{L(t), t \geq 0\}$ is given by

$$\frac{d(L(t))}{dt} = \begin{cases} v^m \text{ if } M(t) = m, \text{and } L(t) > 0, \\ 0, \quad \text{if } L(t) = 0. \end{cases} \tag{13}$$

Note that the "$L(t) = 0$" condition on the last line of Equation (13) follows from the fact that $\{(M(t), L(t)), t \geq 0\}$ is a Markov process with an absorbing barrier at $L(t) = 0$, as a CMT disappears and departs the system if it shrinks to zero length. Define *hitting time* as the random time for a stochastic process to reach a barrier for the first time. The lifetime (τ) of a CMT that appears at time $t = 0$ is given by the hitting time for the length process to reach zero as

$$\tau = \inf\{t > 0 : L(t) = 0\}.$$

We next define a slightly different dynamics for the length process, replacing the condition changing the absorbing barrier at $L(t) = 0$ to a reflective one as follows:

$$\frac{d(L(t))}{dt} = \begin{cases} v^m \text{ if } M(t) = m \in \{GS, GP\}; \text{ or } M(t) = m \in \{SS, SP, PS\}, \text{ and } L(t) > 0, \\ 0, \quad \text{if } M(t) = m \in \{SS, SP, PS\}, \text{ and } L(t) = 0. \end{cases} \tag{14}$$

According to Equation (14), a CMT stays in the system and continues its dynamics even if it shrinks to zero length. That is, once it transitions into a state with a positive net speed, it resumes growth. As the Equations (13) and (14) define similar dynamics up until the first time that a CMT reaches zero length, the lifetime distribution implied by both equations are equivalent. Reformulation in Equation (14) lets us define the lifetime distribution following similar methodology as in Narayanan and Kulkarni (1996). We define the joint distribution function for the lifetime of a CMT and its final state conditioned on the initial state and length as

$$F_{ab}(l,t) = P\{\tau \leq t, M(\tau) = b | L(0) = l, M(0) = a\},$$

where $a, b \in \{GS, GP, SS, SP, PS, PP\}$ represent the initial and final states of the CMT in respective order, and l stands for the initial length. We also define the vector, $F_b(l,t) = [F_{GSb}(l,t) \;\; F_{GPb}(l,t) \;\; F_{SSb}(l,t) \;\; F_{SPb}(l,t) \;\; F_{PSb}(l,t) \;\; F_{PPb}(l,t)]$ for any final state, b. The following theorem states the partial differential equations for this joint distribution function, in terms of the infinitesimal generator matrix Q, and the speed matrix V defined in Section 2,

Theorem 1 *$F_{ab}(l,t)$ is a solution to the following partial differential equation*

$$\frac{\delta F_{ab}(l,t)}{\delta t} - v^a \frac{\delta F_{ab}(l,t)}{\delta l} = \sum_c q_{ac} F_{cb}(l,t), \tag{15}$$

or in the matrix form,

$$\frac{\delta F_b(l,t)}{\delta t} - V \frac{\delta F_b(l,t)}{\delta l} = Q F_b(l,t), \tag{16}$$

where boundary and initial conditions are given by,

$$\begin{aligned}
F_{bb}(0,t) &= 1 \quad \textit{for} \quad v^b < 0, \\
F_{ab}(0,t) &= 0 \quad \textit{for} \quad a \neq b, v^a < 0, \\
F_{ab}(l,0) &= 0 \quad \textit{for} \quad a \neq b, l \geq 0, \\
F_{bb}(l,0) &= 0 \quad \textit{for} \quad l > 0.
\end{aligned}$$

Proof: See Appendix 2. □

Let $F_b^*(l,w)$ be the Laplace transform (LT) of $F_b(l,t)$ with respect to t. We denote the LT of $F_b^*(l,w)$ with respect to l by $F_b^{**}(s,w)$. Next, we give the equations for $F_b^{**}(s,w)$.

Theorem 2 *The solution to Equation (16) in transform space is given by*

$$F_b^{**}(s,w) = (Vs - wI + Q)^{-1}(w^{-1}(Ve_j)),$$

where I is the identity matrix and e_j the j^{th} unit vector, with sizes compatible to V and Q.

Proof: See Appendix 2. □

The transform of the lifetime distribution independent of the final state of the CMT can be stated as

$$F^{**}(s,w) = (Vs - wI + Q)^{-1}(w^{-1}(Ve_3 + Ve_4 + Ve_5)). \tag{17}$$

Note that the reason we multiply V with e_j, where $j = 3, 4, 5$ is that a CMT can only disappear at one of the corresponding states in the set $\{GS, GP, SS, SP, PS, PP\}$ with a negative net speed. We follow the methodology in Kharoufeh and Gautam (2004) to conduct a two-dimensional Laplace transform inversion for numerical computation of $F(l,t)$ for given l and t. For details of the derivation of $F(l,t)$, we refer the reader to Eren (2012).

4.2 Estimation of System Metrics

Next, we conduct a transient analysis to derive the expected number of CMTs in the system according to the lifetime distribution calculated. As CMTs appear according to a Poisson process, and there is no upper bound on CMT number in our model, we can formulate the expected number of CMTs at time t, $E[I(t)]$ similar to the approach in Wolff (1989), where the service time distribution is given by $F(l,t)$. According to this,

$$E[I(t)] = \lambda_a \int_0^t [1 - F(l_0, u)]du, \tag{18}$$

Equation (18) would actually work to approximate only the early phase of simulations, where the interactions are quite rare and ignorable.

In order to compute the integral in Equation (18), we use a summation approximation, based on discrete time points, $t_i = 0, t_1, t_2, ...t_n = t$. Denoting the approximation for $\int_0^{t_i}[1 - F(l_0, u)]du$ by $\widehat{\int}\bar{F}(t_i)$,

$$\widehat{\int}\bar{F}(t_n) = \widehat{\int}\bar{F}(t_{n-1}) + \frac{(F(l_0, t_{n-1}) - F(l_0, t_n))}{2}(t_n - t_{n-1}) + F(l_0, t_n)(t_n - t_{n-1}),$$

for $n = 1, 2, ...$ where $\widehat{\int}\bar{F}(0) = 0$.

The approximation for Equation (18) is given by

$$E[I(t)] \approx \widehat{E}[I(t_n)] = \lambda_a \widehat{\int}\bar{F}(t_n) + I(0)(1 - F(l_0, t_n)). \tag{19}$$

The second term in the right-hand side of Equation (19) is included to account for the possibility of having an initial set of CMTs present in the system at time t, i.e. $I(0) > 0$.

In order to speed up our algorithm, we select intervals such that they get longer for larger t values, since the increment in $F(l_0, t)$ gets quite negligible with increasing t values. More particularly, a CMT has a high disappearance probability early after its appearance as it initially has a tiny length. Given

that it survives, its length grows quickly due to the positive average net velocity common to the parameter sets that we are considering, and the probability of disappearance decreases rapidly.

To estimate $E(\bar{L}(t))$, we do not use the fluid model for the length process, as Equations (13) and (14) are no longer equivalent and would yield different distribution functions of $L(t)$. Instead, we employ a heuristic approach based on simplified simulations for a single CMT with no interactions. Let us denote the approximate expected average length based on these single CMT simulations by $\bar{L}^1(t)$ for different time points $t_i = 0, t_1, t_2..., t_n$ given that a CMT is still in the system at time t. Note that we use thousands of simulations to estimate this average length, which is feasible as single CMT simulations are computationally inexpensive. Defining A_i as the appearance time of CMT i and D_i as its disappearance time, based on the relation

$$E[\bar{L}(t)] = E\left[\frac{\sum_{i=1}^{I(t)} L_i(t)}{I(t)}\right] = E\left[\frac{\sum_{i=1}^{I(t)} L_i(t)|D_i > t, A_i}{I(t)}\right],$$

$E(\bar{L}(t))$ is approximated using the average of the following two estimates where the expected average length and number of CMTs are treated as if independent:

$$\widehat{E}_1[\bar{L}(t_n)] = \frac{\sum_{i=1}^{n} \bar{L}^1(t_n - t_i)\lambda_a(t_i - t_{i-1})(1 - F(t_n - t_i)) + \bar{L}^1(t_n)I(0)(1 - F(t_n))}{\sum_{i=1}^{n} \lambda_a(t_i - t_{i-1})(1 - F(t_n - t_i)) + I(0)(1 - F(t_n))}, \tag{20}$$

and

$$\widehat{E}_2[\bar{L}(t_n)] = \frac{\sum_{i=1}^{n} \bar{L}^1(t_n - t_{i-1})\lambda_a(t_i - t_{i-1})(1 - F(t_n - t_{i-1})) + \bar{L}^1(t_n)I(0)(1 - F(t_n))}{\sum_{i=1}^{n} \lambda_a(t_i - t_{i-1})(1 - F(t_n - t_{i-1})) + I(0)(1 - F(t_n))}, \tag{21}$$

such that

$$E[\bar{L}(t)] \approx \widehat{E}[\bar{L}(t_n)] = \frac{\widehat{E}_1[\bar{L}(t_n)] + \widehat{E}_2[\bar{L}(t_n)]}{2}. \tag{22}$$

According to Equation (20), the CMTs arriving in $[t_i, t_{i+1})$ are assumed to appear in the beginning of the time period, t_i, whereas Equation (21) is based on the assumption that the arrivals in $[t_i, t_{i+1})$ appear at the end of the time period, t_{i+1}. Both equations account for the initially existing CMTs similarly.

Next, we develop two algorithms to adjust the estimations of expected average length and number of CMTs to account for the effects of interactions. The impact of interactions on system metrics is observed to be roughly proportionate to the total length reached in the system during organization, $\widehat{\sum L}$, among different settings with varying input parameters of simulations. This is intuitive as $\widehat{\sum L}$ is a rough measure of crowdedness and density for a given area, which is one of the main determinants of interaction frequency in the system. As a result, we use simulation results for a baseline scenario with a single set of pre-determined parameters to determine weights for smoothing approximations of $E[\bar{L}(t)]$ and $E[I(t)]$ using Algorithm 1 in Appendix 3. For any problem with a new parameter set, only a single simulation is run to roughly

determine the $\widehat{\sum L}$ value at which the system temporarily stabilizes, and its ratio to the corresponding value for the baseline scenario, $\widehat{\sum L}_B$. According to this ratio, β, the weights are adjusted and estimations are calculated using the steps listed in Algorithm 2 in Appendix 3.

4.3 Numerical Results

Having described the proposed methodology for estimation of the expected system metrics, next we compare results obtained with simulations. We first apply Algorithm 1 on the baseline scenario (parameter set I in Appendix 1), and determine weights to be used in Algorithm 2 for other scenarios. Due to space limits, we only present a few examples here, and refer the reader to Eren (2012) for more results.

The set of input parameters for all numerical examples are provided in the Appendix 1. Here, we list the error and control parameters used for the approximations and algorithms. For the approximations in Equations (19) and (22), we use time points $t = 0, 0.25, 0.5, 1, 2, ...$ (note that intervals get larger for higher t values as explained in Section 4.2). For Algorithm 1, we set $\rho_L^c = 0.02$, $\rho_L^q = 0.01$, $\rho_I^c = 0.04$, $\rho_I^q = 0.03$, based on our trials with various values. According to this, the fitted values (dark solid line) for the baseline scenario along with results of 10 independent simulation runs (jagged light lines) are plotted in Figure 8. This case is used to estimate weights δ_t, γ_t and corresponding total length ($L_B(t)$) values to be fed into Algorithm 2 to calculate estimations for the remaining scenarios.

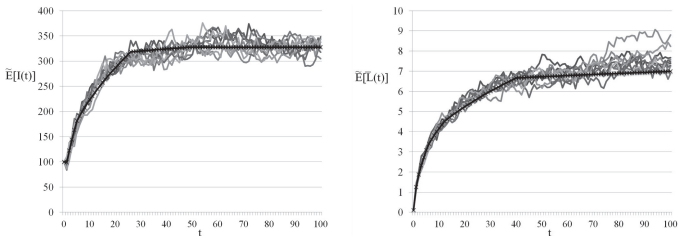

Fig. 8 10 Independent Realizations of the Baseline Scenario (Parameter Set I) with Fitted Values

Having calculated the weights (for estimation) using simulation results of the baseline scenario, we follow with implementation of the prediction algorithm on the other parameter sets. First we present two highly dynamic cases, given by parameter sets II and III. For set II, $\beta \approx 2.2$, which implies that the total system length is roughly 2.2 times that of the baseline case around the time organization settles. For set III, the system gets even more crowded ($\beta \approx 6.1$). Resulting estimations together with 10 independent realizations from simulations are provided in Figures 9 and 10. The estimations of our

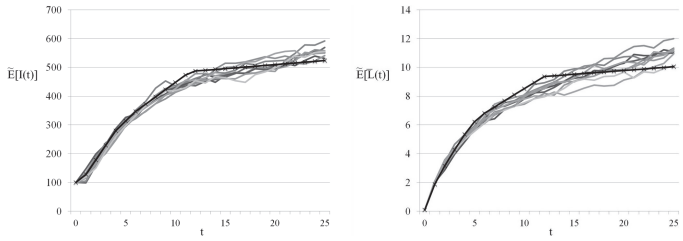

Fig. 9 Estimations for $\beta \approx 2.2$ case

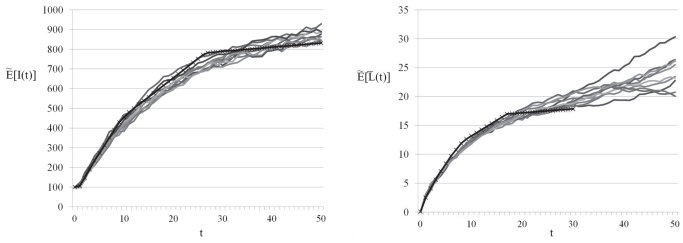

Fig. 10 Estimations for $\beta \approx 6.1$ case

proposed method seem to stay around the range of simulation results. Due to the highly dynamic nature of both cases, organization occurs quite rapidly, and the pseudo-stabilization of system metrics last for a very short time. Further, as seen in Figures 9 and 10, metrics continue to slowly increase rather than completely stabilizing while organization settles. However, the proposed methodology still captures the average trend over time.

We continue with another numerical example, where we use a parameter set that is relatively less dynamic, obtained by reducing the dynamicity parameters and appearance rate of the baseline data set by half. The resulting β value is 0.95 and estimations are provided in Figure 11. Note that the total length reached in this case (as well as the average length and total number of CMTs) is quite close to that of the baseline scenario even though the dynamicity and appearance rate of CMTs are reduced by half in this case. This is quite intuitive, as the system stabilizes around a point where the arrival process and length dynamics balance each other. However, timewise, it is observed that having a less dynamic system delays organization, as evidenced by the duration it takes to reach quasi-stabilization relative to the baseline case. Finally, in Figure 12, we present a case with different interaction parameters ($p_b = 0.5$, $p_c = 0.6$, $\theta^c = 60^0$) with respect to the baseline scenario and a β value of 0.95, and see that estimations are pretty close to the simulation results for that case as well.

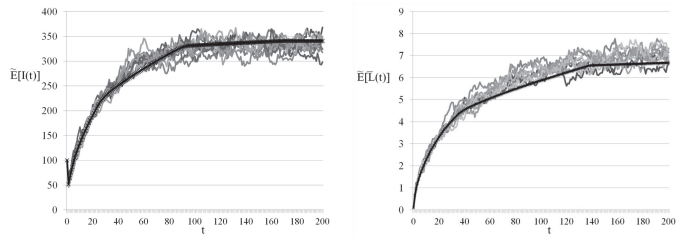

Fig. 11 Estimations for $\beta \approx 0.95$ case

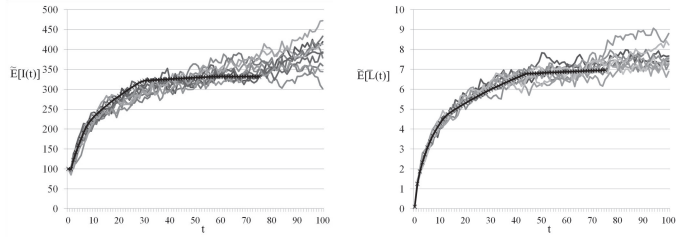

Fig. 12 Estimations for $\beta \approx 0.95$ case (with different interaction parameters)

5 Discussion and Concluding Remarks

In this paper, we studied the self-organization of CMTs into linearly ordered arrays, which are important for the morphogenesis of plant cells. Due to the spatio-temporal nature of the stochastic dynamics and interactions of CMTs, these arrays are challenging to analyze. By combining a range of methodologies, we were able to model the organization and important structural metrics of this complex system in ways that would have been prohibitive or impossible using real experiments. In particular, we derived a simple condition using a mean-field model that can be used to instantaneously check if a set of input parameters would result in organization. Likewise, our predictive algorithms enable efficient estimation of system metrics such as number and length of CMTs, which are difficult to measure experimentally because of the highly bundled and crowded organization of CMT arrays. Figure 13 provides a flow chart that summarizes the use of the developed methodologies in this study.

Our analytical models are able to reproduce results that were derived from an earlier simulation study (Eren et al, 2010). This serves to validate the developed models since the simulations were confirmed to mimic known CMT system properties such as average length of CMTs, expected time frame for organization, and abnormal CMT arrays observed in mutant plants (Eren et al, 2010). Thus, by comparing analytical results obtained directly to simulations, we are able to conclude that the derived methodologies can be used as a

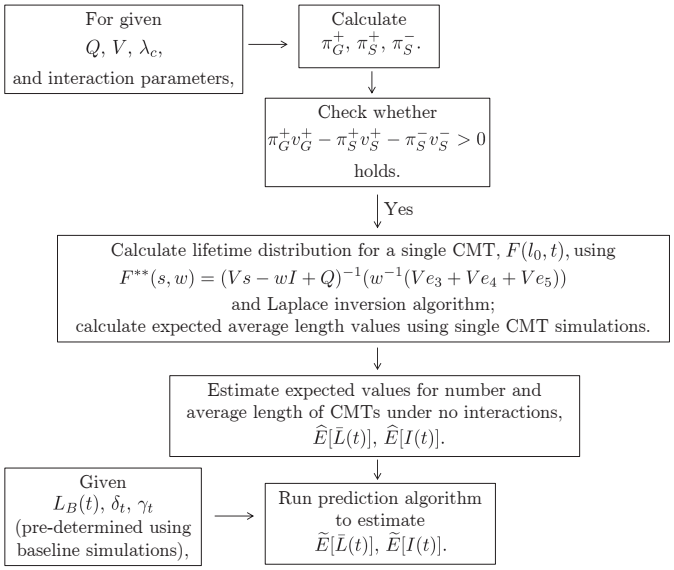

Fig. 13 Flowchart for Estimation of System Metrics for a Given Set of Input Parameters

valid representation of real plant cell systems. Moreover, the analytical models helped us generalize and explore the underpinnings of certain findings from the simulation study such as the significance of proper dynamicity parameters and the role of interactions between CMTs.

Our analytical methodologies also provided new biological insights that would have been difficult to capture or generalize in real plant experiments. Specifically, we observed that nature has selected parameters that ensure that CMT organization occurs robustly (i.e. organization is independent of the interaction parameters as long as the dynamics are in a growth-prone range), while also allowing for array reorganization to occur in response to developmental and environmental signals (as implied by the different array structures that emerge with different parameters). The tubulin subunit levels in plant cells appear to be selected so that they are just sufficient for organization (i.e. to reach to the crowdedness at around quasi-stabilization phase), but also constraining enough to prevent overproduction of CMTs (as seen in extended simulations with no tubulin limit), which might hinder array organization and impede array reorganization. Using our estimation methodology, we calculate the tubulin dimer concentration at the cortex of plant cells to be roughly 10-20 micromolar. As new measuring technologies emerge, if this parameter becomes available as an input, our predictive approach can be improved to eliminate

its reliance on a single simulation run for each scenario with a given parameter set.

Overall, our analytical methods provide new tools to predict important system properties based on input parameters related to individual CMT dynamics and interactions, which can also be used to engineer settings to maintain and control organization. These methodologies can be applied to similar noncentrosomal microtubule arrays that are found in specialized animal cells such as neurons and muscle cells, where ordered arrays are critical for the specialized morphology and functions. This research is also related to the field of biofuel engineering, as CMT organization directly influences the ordered deposition of cellulose microfibrils, the most abundant biopolymer on the planet. Finally, our work has implications for the design and assembly of microtubule-inspired nanostructures for the directional transport of material (Goel and Vogel, 2008).

Finally, we note some limitations of our study and opportunities for future work. Some immediate extensions would be consideration of continuous angles and multiple CMT systems for the mean-field model. Although we capture the alignment and density of CMTs in our analytical models, other features of CMT arrays such as polarity and overall orientation with respect to the cell axis are not incorporated. While the latter aspects can be easily included in computer simulations (Eren et al, 2010), considering them in analytical models is more challenging as they require formulation of system coordinates. Furthermore, mechanical stress fields and their impact on CMT orientation are additional components to consider, since these are important biologically (Hamant et al, 2008). As the models are extended to include further aspects of array structure, the quantification metrics must also be improved to capture these properties.

References

Allard JF, Wasteneys GO, Cytrynbaum EN (2010) Mechanisms of Self-organization of Cortical Microtubules in Plants Revealed by Computational Simulations. Molecular Biology of the Cell 21(2):278–286

Barton DA, Vantard M, Overall RL (2008) Analysis of Cortical Arrays from Tradescantia Virginiana at High Resolution Reveals Discrete Microtubule Subpopulations and Demonstrates That Confocal Images of Arrays Can Be Misleading. Plant Cell 20:982–994

Baulin VA, Marques CM, Thalmann F (2007) Collision Induced Spatial Organization of Microtubules. Biophysical Chemistry 128(2-3):231–244

Burk DH, Ye ZH (2002) Alteration of Oriented Deposition of Cellulose Microfibrils by Mutation of a Katanin-Like Microtubule-Severing Protein. Plant Cell 14(9):2145–2160

Burk DH, Liu B, Zhong R, Morrison WH, Ye ZH (2001) A Katanin-Like Protein Regulates Normal Cell Wall Biosynthesis and Cell Elongation. Plant Cell 13(4):807–827

Deinum EE, Tindemans SH, Mulder BM (2011) Taking Directions: The Role of Microtubule-Bound Nucleation in the Self-Organization of the Plant Cortical Array. Physical Biology 8(5):056,002

Dixit R, Cyr R (2004a) Encounters Between Dynamic Cortical Microtubules Promote Ordering of the Cortical Array through Angle-Dependent Modifications of Microtubule Behavior. Plant Cell 16(12):3274–3284

Dixit R, Cyr R (2004b) The Cortical Microtubule Array: From Dynamics to Organization. Plant Cell 16(10):2546–2552

Dixit R, Chang E, Cyr R (2006) Establishment of Polarity During Organization of the Acentrosomal Plant Cortical Microtubule Array. Molecular Biology of the Cell 17(3):1298–1305

Dogterom M, Leibler S (1993) Physical Aspects of the Growth and Regulation of Microtubule Structures. Physical Review Letters 70(9):1347–1350

Ehrhardt DW, Shaw SL (2006) Microtubule Dynamics and Organization in the Plant Cortical Array. Annual Review of Plant Biology 57:859–875

Eren EC (2012) Stochastic modeling and analysis of plant microtubule system characteristics. PhD thesis, Texas A&M University, College Station, TX

Eren EC, Dixit R, Gautam N (2010) A Three-Dimensional Computer Simulation Model Reveals the Mechanisms for Self-Organization of Plant Cortical Microtubules into Oblique Arrays. Molecular Biology of the Cell 21(15):2674–2684

Eren EC, Gautam N, Dixit R (2012) Computer Simulation and Mathematical Models of the Noncentrosomal Plant Cortical Microtubule Cytoskeleton. Cytoskeleton p 10.1002/cm.21009

Goel A, Vogel V (2008) Harnessing Biological Motors to Engineer Systems for Nanoscale Transport and Assembly. Nature Nanotechnology 3(8):465–475

Gray RM (1990) Entropy and Information Theory. Springer-Verlag, New York

Hamant O, Heisler MG, Jonsson H, Krupinski P, Uyttewaal M, Bokov P, Corson F, Sahlin P, Boudaoud A, Meyerowitz EM, et al (2008) Developmental Patterning by Mechanical Signals in Arabidopsis. Science 322(5908):1650–1655

Hardham AR, Gunning BE (1978) Structure of Cortical Microtubule Arrays in Plant Cells. Journal of Cell Biology 77:14–34

Hawkins RJ, Tindemans SH, Mulder BM (2010) Model for the Orientational Ordering of the Plant Microtubule Cortical Array. Physical Review E 82(1 Pt 1):011,911

Ishida T, Kaneko Y, Iwano M, Hashimoto T (2007) Helical Microtubule Arrays in a Collection of Twisting Tubulin Mutants of Arabidopsis Thaliana. Proceedings of the National Academy of Sciences of the United States of America 104(20):8544–8549

Kawamura E, Wasteneys GO (2008) MOR1, the Arabidopsis Thaliana Homologue of Xenopus MAP215, Promotes Rapid Growth and Shrinkage, and Suppresses the Pausing of Microtubules in Vivo. Journal of Cell Science 121(24):4114–4123

Khalil HK (2002) Nonlinear Systems. Prentice Hall, Upper Saddle River, NJ

Kharoufeh JP, Gautam N (2004) Deriving Link Travel-Time Distributions Via Stochastic Speed Processes. Transportation Science 38(1):97–106

Long EF, Vaidya NK, Brandeau ML (2008) Controlling Co-Epidemics: Analysis of HIV and Tuberclosis Infection Dynamics. Operations Research 56(6):1366–1381

Lu JL, Valois F, Dohler M, Barthel D (2008) Quantifying Organization by Means of Entropy. IEEE Communications Letters 12(3):185–187

Martin MT, Plastinoa A, Rossob OA (2006) Generalized Statistical Complexity Measures: Geometrical and Analytical Properties. Physica A 369(2):439–462

Narayanan A, Kulkarni VG (1996) First passage times in fluid models with an application to two priority fluid systems. In: Proceedings of the 2nd International Computer Performance and Dependability Symposium, IEEE, Washington, DC, pp 166–175

Shannon CE (1948) A Mathematical Theory of Communication. The Bell System Technical Journal 27:379–423

Shaw SL, Kamyar R, Ehrhardt DW (2003) Sustained Microtubule Treadmilling in Arabidopsis Cortical Arrays. Science 300(5626):1715–1718

Shi X, Ma Y (2010) Understanding Phase Behavior of Plant Cell Cortex Microtubule Organization. Proceedings of the National Academy of Sciences 107(26):11,709–11,714

Tindemans SH, Hawkins RJ, Mulder BM (2010) Survival of the Aligned: Ordering of the Plant Cortical Microtubule Array. Physical Review Letters 104(5):058,103

Vos JW, Dogterom M, Emons AMC (2004) Microtubules Become More Dynamic But Not Shorter During Preprophase Band Formation: A Possible "Search-and-Capture" Mechanism for Microtubule Translocation. Cell Motility and the Cytoskeleton 57:246–258

Wasteneys GO, Ambrose JC (2009) Spatial Organization of Plant Cortical Microtubules: Close Encounters of the 2D Kind. Trends in Cell Biology 19(2):62–71

Wolff RW (1989) Stochastic Modeling and the Theory of Queues. Prentice Hall, New Jersey

Zhang Q, Fishel EA, Bertroche T, Dixit R (2013) Microtubule Severing at Crossover Sites by Katanin Generates Ordered Cortical Microtubule Arrays in Arabidopsis. Current Biology 23:2191–2195

Appendix 1: Input Parameter Sets (Dynamics)

$Q = [q_{m,n}]$, $m, n \in \{GS, GP, SS, SP, PS, PP\}$
$V = diag(v^m)$, $m \in \{GS, GP, SS, SP, PS, PP\}$
Parameter Set I:

$$Q = \begin{bmatrix} -8.925 & 6.72 & 1.485 & 0 & 0.72 & 0 \\ 2.427 & -4.632 & 0 & 1.485 & 0 & 0.72 \\ 3.537 & 0 & -11.192 & 6.72 & 0.935 & 0 \\ 0 & 3.537 & 2.427 & -6.898 & 0 & 0.935 \\ 5.05 & 0 & 2.376 & 0 & -14.1 & 6.72 \\ 0 & 5.05 & 0 & 2.376 & 2.427 & -9.85 \end{bmatrix}.$$

$$V = diag(0.91, 3.69, -8.66, -5.88, -2.78, 0)$$

Parameter Set II:

$$Q = \begin{bmatrix} -7.234 & 6.72 & 0.236 & 0 & 0.278 & 0 \\ 2.427 & -2.941 & 0 & 0.236 & 0 & 0.278 \\ 5 & 0 & -13.27 & 6.72 & 1.55 & 0 \\ 0 & 5 & 2.427 & -8.977 & 0 & 1.55 \\ 25.125 & 0 & 12.75 & 0 & -44.595 & 6.72 \\ 0 & 25.125 & 0 & 12.75 & 2.427 & -40.302 \end{bmatrix}$$

$$V = diag(0.72, 3.5, -11.78, -9, -2.78, 0)$$

Parameter Set III:

$$Q = \begin{bmatrix} -9.617 & 6.72 & 2.338 & 0 & 0.559 & 0 \\ 2.427 & -5.324 & 0 & 2.338 & 0 & 0.559 \\ 12.438 & 0 & -21.908 & 6.72 & 2.75 & 0 \\ 0 & 12.438 & 2.427 & -17.614 & 0 & 2.75 \\ 8.75 & 0 & 4.375 & 0 & -19.845 & 6.72 \\ 0 & 8.75 & 0 & 4.375 & 2.427 & -15.552 \end{bmatrix}$$

$$V = diag(3.72, 6.5, -15.18, -12.4, -2.78, 0)$$

Parameter Set IV:

$$Q = \begin{bmatrix} -7.537 & 6.72 & 0.535 & 0 & 0.282 & 0 \\ 2.427 & -3.244 & 0 & 0.53521 & 0 & 0.282 \\ 6.211 & 0 & -16.036 & 6.72 & 3.105 & 0 \\ 0 & 6.211 & 2.427 & -11.742 & 0 & 3.105 \\ 15.6 & 0 & 5.6 & 0 & -27.92 & 6.72 \\ 0 & 15.6 & 0 & 5.6 & 2.427 & -23.627 \end{bmatrix}$$

$$V = diag(-0.28, 2.5, -8.98, -6.2, -2.78, 0)$$

Parameter Set V:

$$Q = \begin{bmatrix} -11.806 & 6.72 & 2.343 & 0 & 2.743 & 0 \\ 2.427 & -7.512 & 0 & 2.343 & 0 & 2.743 \\ 3.05 & 0 & -15.82 & 6.72 & 6.05 & 0 \\ 0 & 3.05 & 2.427 & -11.527 & 0 & 6.05 \\ 1.556 & 0 & 1.378 & 0 & -9.653 & 6.72 \\ 0 & 1.556 & 0 & 1.378 & 2.427 & -5.36 \end{bmatrix}$$

$$V = diag(-0.78, 2, -6.58, -3.8, -2.78, 0)$$

Parameter Set VI:

$$Q = \begin{bmatrix} -8.925 & 6.72 & 1.485 & 0 & 0.72 & 0 \\ 2.427 & -4.632 & 0 & 1.485 & 0 & 0.72 \\ 3.537 & 0 & -11.192 & 6.72 & 0.935 & 0 \\ 0 & 3.537 & 2.427 & -6.898 & 0 & 0.935 \\ 5.05 & 0 & 2.376 & 0 & -14.1 & 6.72 \\ 0 & 5.05 & 0 & 2.376 & 2.427 & -9.85 \end{bmatrix}.$$

$$V = diag(3.69, 3.69, -5.88, -5.88, 0, 0)$$

Appendix 2: Proofs

Lemma 1
Let us define $z_i = (y_i - x_i)$ $i = 1, ..., N$. We group z_i values in three sets as follows:

$$I_+ = \{i \in \{1, N\} : z_i > 0\}$$
$$I_0 = \{i \in \{1, N\} : z_i = 0\}$$
$$I_- = \{i \in \{1, N\} : z_i < 0\}.$$

As $\sum_{i=1}^{N} y_i - \sum_{i=1}^{N} x_i = 0$, it follows that

$$\sum_{i=1}^{N} z_i = \sum_{i \in I_+} z_i + \sum_{i \in I_-} z_i = 0. \tag{23}$$

Let us divide z_i values into infinitesimal pieces of the same size, denoted by $\Delta_z > 0$, such that for each $i \in I_+$, $z_i = w_i \Delta_z$ and for each $i \in I_-$, $z_i = -w_i \Delta_z$, $i = 1, ..., N$, where $\Delta_z > 0$ and w_i are positive real numbers. Equation (23) can be rewritten as

$$\sum_{i \in I_+} w_i - \sum_{i \in I_-} w_i = 0. \tag{24}$$

Hence, we have an equal number ($\sum_{i\in I_+} w_i = \sum_{i\in I_-} w_i := W$) of Δ_z pieces that belong to sets I_+ and I_-. Note that $\forall\ z_i$ with $i \in I_+$ and z_j with $j \in I_-$, it follows from the definition of z_i values that $z_i > z_j$, and consequently $x_i > x_j$ from the given ordering relation between the sequences x_i, and z_i; and finally $f(x_i) < f(x_j)$ due to the decreasing property of $f(\cdot)$. Let us redefine the sequence of x_i, $i = 1, ..., N$ such that its values are copied w_i times for each x_i value so that every Δ_z has its corresponding $x'_{i'}$ and $f(x'_{i'})$ values, where $i' = 1, ..., W$. Adjusting I_+ and I_- accordingly as I'_+, I'_-, for each Δ_z value that belongs to set I_+, there is a Δ_z which is multiplied with a larger value in I_- in the following equation:

$$\sum_{i'\in I'_+} f(x'_{i'})\Delta_z - \sum_{i'\in I'_-} f(x'_{i'})\Delta_z < 0,$$

which gives the desired result.

Proposition 1

According to Lyapunov's stability theory, a sufficient condition for the global asymptotic stability of an equilibrium point P^* is existence of a Lyapunov function $\mathcal{L}(\cdot)$ such that

- $\mathcal{L}(t)\mid_P > 0$, $\forall P \neq P^*$ and $\mathcal{L}(t)\mid_P = 0$ only for $P = P^*$,
- $\frac{\partial \mathcal{L}(t)}{\partial t}\mid_P < 0$, $\forall P \neq P^*$ and $\frac{\partial \mathcal{L}(t)}{\partial t}\mid_{P=P^*} = 0$.

We set our Lyapunov function as the entropy metric, $H(\cdot)$ in Equation (**??**). We already know that the first condition holds for $H(\cdot)$, as $H(t)\mid_{P=P^*} = 0$ and $H(t)\mid_P > 0\ \forall P \neq P^*$. What is left to check is the sign of the derivative of the Lyapunov function with respect to t, which is given by

$$\frac{\partial H(t)}{\partial t} = -\sum_{\theta=0}^{179} k'(\theta,t) ln(k(\theta,t)) + k'(\theta,t), \tag{25}$$

where

$$k'(\theta,t) = \frac{\partial\ k(\theta,t)}{\partial t}. \tag{26}$$

Let us define the total density of CMTs with length l and angle θ at time t by

$$\bar{p}(l,\theta,t) := \bar{p}_G(l,\theta,t) + \bar{p}_S(l,\theta,t) + \bar{p}_P(l,\theta,t).$$

Using Equation (10), we can rewrite Equation (26) as

$$k'(\theta,t) = \frac{\left(\int_0^\infty l\frac{d\bar{p}(l,\theta,t)}{dt}dl\right)\sum_{\theta=0}^{179}\int_0^\infty l\bar{p}(l,\theta,t)dl - \left(\int_0^\infty l\bar{p}(l,\theta,t)dl\right)\sum_{\theta=0}^{179}\int_0^\infty l\frac{d\bar{p}(l,\theta,t)}{dt}dl}{\left(\sum_{\theta=0}^{179}\int_0^\infty l\bar{p}(l,\theta,t)dl\right)^2}.$$

Summing equations in (5) side by side, multiplying both sides with l and integrating with respect to l over $(0,\infty)$, we obtain the derivative of total

length of all CMTs with angle θ at time t as

$$\begin{aligned} L'_\theta(t) &:= \int_0^\infty l \frac{d\bar{p}(l,\theta,t)}{dt} dl \\ &= (v_G^+ - v_S^-)\tilde{p}_{GS}(\theta,t) + v_G^+ \tilde{p}_{GP}(\theta,t) \\ &- (v_S^+ + v_S^-)\tilde{p}_{SS}(\theta,t) - v_S^+ \tilde{p}_{SP}(\theta,t) - v_S^- \tilde{p}_{PS}(\theta,t) \\ &- v_G^+ \int_0^\infty \bar{p}_G(l,\theta,t) l dl \sum_{\theta' \in \Theta^*} p_b |sin(\theta - \theta')| \int_{l'} dl' l' \bar{p}(l',\theta',t) \\ &+ v_G^+ \int_{l'} dl' l' \bar{p}(l',\theta,t) \sum_{\theta' \in \Theta^*} p_b |sin(\theta - \theta') \int_0^\infty \bar{p}_G(l,\theta',t) l dl, \end{aligned}$$

where $\tilde{p}_m(\theta,t) := \int_0^\infty p_m(l,\theta,t)dl$, $m \in \{GS, GP, SS, SP, PS, PP\}$ stands for the total density of CMTs with angle θ at state m at time t. We denote the sum of $L'_\theta(t)$ over all θ by $\sum L'(t) := \sum_{\theta=0}^{179} L'_\theta(t)$, which gives the derivative of total length of all CMTs in the system at time t. Defining total length of CMTs with angle θ at time t as $L_\theta(t) := \int_0^\infty lp(l,\theta,t)dl$, and the total length of all CMTs at time t as $\sum L(t) := \sum_{\theta=1}^{360} L_\theta(t)$, and plugging these into Equation (25) results in

$$\frac{dH(t)}{dt} = -\sum_{\theta=0}^{179} \frac{L'_\theta(t) \ln\left(\frac{L_\theta(t)}{\sum L(t)}\right) \sum L(t) - L_\theta(t) \ln\left(\frac{L_\theta(t)}{\sum L(t)}\right) \sum L'(t)}{(\sum L(t))^2}.$$

Rearranging terms, we obtain

$$\frac{dH(t)}{dt} = -\sum_{\theta=0}^{179} \frac{\frac{L'_\theta(t)}{\sum L'(t)} \ln\left(\frac{L_\theta(t)}{\sum L(t)}\right) - \frac{L_\theta(t)}{\sum L(t)} \ln\left(\frac{L_\theta(t)}{\sum L(t)}\right)}{\sum L(t) \sum L'(t)}. \tag{27}$$

Let us denote $a_\theta := \frac{L'_\theta(t)}{\sum L'(t)}$ and $b_\theta := \frac{L_\theta(t)}{\sum L(t)}$. By definition, it follows that $\sum_{\theta=0}^{179} a_\theta = 1$, $\sum_{\theta=0}^{179} b_\theta = 1$, and $b_i > 0$. Assuming $\sum L'(t) > 0$, i.e. the net total CMT length change in time is positive, we are interested in the sign of

$$\sum - \ln(b_\theta)(a_\theta - b_\theta). \tag{28}$$

If the sign for Expression (28) is negative, then Equation (27) is negative, i.e. $\frac{dH}{dt} < 0$, and the stability condition is satisfied. A sufficient condition to ensure this follows from Lemma 1 as $-ln(b)$ is a decreasing function of b for $0 < b < 1$. Accordingly, we require the two sequences a_θ and b_θ, and their difference $a_\theta - b_\theta$ to increase and decrease in the same order. This roughly means that if CMTs with an angle θ have a larger total length compared to the total length of CMTs with angle $\theta' \neq \theta$, they also grow larger in ratio in total length on average, and vice versa. This property follows by careful observation of model equations and the property that $p_b(l)$ is decreasing in l.

Finally, in order to fulfill $\sum L'(t) > 0$, it is required that the problem parameters satisfy

$$\sum_{\theta}(v_G^+ - v_S^-)p_{GS}(\theta,t) + v_G^+ p_{GP}(\theta,t) - (v_S^+ + v_S^-)p_{SS}(\theta,t) - v_S^+ p_{SP}(\theta,t) - v_S^- p_{PS}(\theta,t) > 0, \ , \tag{29}$$

$\forall t$, which can be stated as

$$\sum_{\theta} p_G^+(\theta,t)v_{G^+} - p_S^+(\theta,t)v_{S^+} - p_S^-(\theta,t)v_{S^-} > 0, \tag{30}$$

by rearranging terms.

Theorem 1

Consider $F_{ab}(l, t+h)$, where h is a small positive real number. It can be written as

$$F_{ab}(l,t+h) = P\{\tau \le t+h, M(\tau) = b | L(0) = l, M(0) = a\}.$$

Conditioning on the first transition from the initial state, we obtain

$$\begin{aligned} F_{ab}(l,t+h) =& P\{\tau \le t+h, M(\tau) = b | L(0) = l, M(0) = a\} \\ =& \sum_{c \ne a} P\{\tau \le t+h, M(\tau) = b | L(0) = l, M(0) = a, M(h) = c\} \\ & \quad P\{M(h) = c | M(0) = a, L(0) = l\} \\ & + P\{\tau \le t+h, M(\tau) = b | L(0) = l, M(0) = a, M(h) = a\} \\ & \quad P\{M(h) = a | M(0) = a, L(0) = l\}. \end{aligned}$$

As $M(t)$ process is independent of $L(0)$, and the length would change by $v^a h$ by time h, when the CMT is in state a at time 0,

$$\begin{aligned} & F_{ab}(l,t+h) \\ =& \sum_{c \ne a} P\{\tau \le t+h, M(\tau) = b | L(h) = l + v^a h, M(h) = c\} P\{M(h) = c | M(0) = a\} \\ & + P\{\tau \le t+h, M(\tau) = b | L(h) = l + v^a h, M(h) = a\} P\{M(h) = a | M(0) = a\} \\ =& \sum_{c \ne a} P\{\tau \le t, M(\tau) = b | L(0) = l + v^a h, M(0) = c\} P\{M(h) = c | M(0) = a\} \\ & + P\{\tau \le t, M(\tau) = b | L(0) = l + v^a h, M(0) = a\} P\{M(h) = a | M(0) = a\}. \end{aligned}$$

As the transition probability from state a to c in time h is given by $q_{ac}h + o(h)$ if $c \ne a$ and $1 + q_{aa}h + o(h)$ if $c = a$, where $o(h)$ is a collection of terms of higher order than h such that $o(h)/h \to 0$ as $h \to 0$, it follows

$$F_{ab}(l,t+h) = \sum_{c \ne a} F_{cb}(l + v^a h, t) q_{ac} h + F_{ab}(l + v^a h, t)(q_{aa}h + 1) + o(h).$$

Subtracting $F_{ab}(l,t)$ from each side of the equation, dividing by h and rearranging terms results in

$$\frac{F_{ab}(l,t+h) - F_{ab}(l,t)}{h} = \frac{F_{ab}(l + v^a h, t) - F_{ab}(l,t)}{h} + \sum_c q_{ac} F_{cb}(l + v^a h, t) + o(h)/h.$$

Letting $h \to 0$ yields Equation (15), and rewriting in the matrix form gives Equation (16). Next, we describe the boundary conditions for all a, b and t. As the lifetime would be zero if CMT appeared with zero length at state b such that $v^b < 0$, it follows

$$F_{bb}(0,t) = 1 \quad \text{for} \quad v^b < 0.$$

The second boundary condition,

$$F_{ab}(0,t) = 0 \quad \text{for} \quad a \neq b, v^a < 0,$$

follows from the fact that although the lifetime is zero, the probability that the state is b when the lifetime is reached is zero (since at time $t = 0$ the state is a with $v^a < 0$). Finally, the last two conditions follow from the fact that lifetime cannot be reached at state b at time $t = 0$ if the initial state is $a \neq b$ for any initial length; or if the initial state is b for a positive initial length.

Theorem 2

Taking the LT of Equation (16) with respect to t gives

$$(wI - Q)F_b^*(l,w) = V\frac{\delta F_b^*(l,w)}{\delta l}. \tag{31}$$

Taking the LT of Equation (31) with respect to l results in

$$(wI - Q)F_b^{**}(s,w) = V[sF_b^{**}(s,w) - F_b^*(0,w)]. \tag{32}$$

Define e_j as the j^{th} unit vector. Plugging in the boundary condition

$$F_b^*(0,w) = w^{-1}e_j \quad if \quad v^j < 0,$$

we get

$$(Vs - wI + Q)\tilde{F}_b^*(s,w) = w^{-1}(Ve_j).$$

Rearranging terms yields Equation (17).

Appendix 3: Algorithms for Estimation of System Metrics

Algorithm 1 *(Determination of weights)*
0: Run R independent simulations of the baseline setting to obtain R realizations of both system metrics: $\bar{L}_r(t)$, $I_r(t)$, $r = 1, ..., R$, $t = 1, ..., T$. Calculate their minimum, maximum, and average values among independent runs, $\min_r \bar{L}_r(t)$, $\min_r I_r(t)$; $\max_r \bar{L}_r(t)$, $\max_r I_r(t)$; $\bar{\bar{L}}(t)$, $\bar{I}(t)$ respectively for $t = 1, ..., T$. Note that the total length in the system reaches $\widehat{\sum L}$ at time T.
1: Set the initial weight for $E[\bar{L}(t)]$, $\delta_1 = 1$ and the one for $E[I(t)]$, $\gamma_1 = 1$, and error check and control parameters for both metrics, $\rho_L^c, \rho_I^c, \rho_L^g, \rho_I^g$.
2: Initialize estimations $\widetilde{E}[\bar{L}(1)] = \widehat{E}[\bar{L}(1)]$, $\widetilde{E}[I(1)] = \widehat{E}[I(1)]$, and $\widetilde{\sum} L(1) = \widetilde{E}[\bar{L}(1)]\widetilde{E}[I(1)]$; and the vector used to store the total length values corresponding to the base weights calculated in this algorithm, $L_B(1) = 1$.

3: FOR $t = 1$ *TO* T
4: $\widetilde{E}[\bar{L}(t+1)] = \widetilde{E}[\bar{L}(t)] + \delta_t(\widehat{E}[\bar{L}(t+1)] - \widehat{E}[\bar{L}(t)])$
5: $\rho_L = \frac{\widetilde{E}[\bar{L}(t+1)] - \bar{\bar{L}}(t+1)}{\bar{\bar{L}}(t+1)}$ *//Calculate deviation from the average.*
6: IF $\rho_L < \rho_L^c$ *AND* $\min_r \bar{L}(t+1) < \widetilde{E}[\bar{L}(t+1)] < \max_r \bar{L}(t+1)$ *//Check if deviation is lower than the critical value and if the estimation is in the range between the minimum and maximum of realizations.*
7: $\delta_{t+1} = \delta_t$
8: ELSE
9: WHILE ($\rho_L > \rho_L^c$ *OR* $\widetilde{E}[\bar{L}(t+1)] > \max_r \bar{L}(t+1)$) *AND* $\delta_{t+1} > 0.05$
10: $\delta_{t+1} = \delta_{t+1} - 0.05$ *//Update weight.*
11: $\widetilde{E}[\bar{L}(t+1)] = \widetilde{E}[\bar{L}(t)] + \delta_{t+1}(\widehat{E}[\bar{L}(t+1)] - \widehat{E}[\bar{L}(t)])$ *//Update estimation.*
12: $\rho_L = \frac{\widetilde{E}[\bar{L}(t+1)] - \bar{\bar{L}}(t+1)}{\bar{\bar{L}}(t+1)}$ *//Update deviation from average.*
13: END WHILE
14: END IF
15: Repeat similar cycle (steps 4-14) for estimating $\widetilde{E}[I(t+1)]$ *and* γ_{t+1}.
16: $\widetilde{\sum} L(t+1) = \widetilde{E}[\bar{L}(t+1)]\widetilde{E}[I(t+1)]$ *//Calculate the estimated total length.*
17: $L_B(t+1) = \widetilde{\sum} L(t+1)$ *//Store the total length values corresponding to the weights.*
18: END FOR

Algorithm 2 *(Prediction algorithm)*
0: Calculate $\beta = \frac{\widehat{\sum} L}{\widehat{\sum} L_B}$ *//Ratio of total length capacity to that of the baseline.*
1: Initialize estimations $\widetilde{E}[\bar{L}(1)] = \widehat{E}[\bar{L}(1)]$, $\widetilde{E}[I(1)] = \widehat{E}[I(1)]$, *and* $\widetilde{\sum} L(1) = \widetilde{E}[\bar{L}(1)]\widetilde{E}[I(1)]$; *weights for estimations* $w_L = w_I = 1$ *and positions for these weights* $p_L, p_I = 1$ *in the pre-determined weight vectors (see Algorithm 1).*
2: FOR $t = 1$ *TO* T' *//A maximum time point for estimations.*
3: IF $\widetilde{\sum} L(t) < \widehat{\sum} L$ *//Total length cap not exceeded.*
4: $\widetilde{E}[\bar{L}(t+1)] = \widetilde{E}[\bar{L}(t)] + w_L(\widehat{E}[\bar{L}(t+1)] - \widehat{E}[\bar{L}(t)])$
5: $\widetilde{E}[I(t+1)] = \widetilde{E}[I(t)] + w_I(\widehat{E}[I(t+1)] - \widehat{E}[I(t)])$
6: ELSE
7: $\widetilde{E}[\bar{L}(t+1)] = \widetilde{E}[\bar{L}(t)]$; $\widetilde{E}[I(t+1)] = \widetilde{E}[I(t)]$.
8: END IF
9: $\widetilde{\sum} L(t+1) = \widetilde{E}[I(t+1)]\widetilde{E}[\bar{L}(t+1)]$
10: FOR $u = p_L : T_{max}$
11: IF $\widetilde{\sum} L(t+1) > \beta L_B(u)$ *//Updates weights if required comparing total length values to the pre-calculated base values (Algorithm 1).*
12: $w_L = \delta(u), p_L = u$ *//Update weights and position in the base vector.*
13: $\widetilde{E}[\bar{L}(t+1)] = \widetilde{E}[\bar{L}(t)] + w_L(\widehat{E}[\bar{L}(t+1)] - \widehat{E}[\bar{L}(t)])$ *//Update estimation.*
14: END IF

15: END FOR
16: $\widetilde{E}[\bar{L}(t+1)] = \widetilde{E}[\bar{L}(t)] + w_L(\widehat{E}[\bar{L}(t+1)] - \widehat{E}[\bar{L}(t)])$
17: Repeat Steps 10-15 similarly for w_I, p_I *and* $\widetilde{E}[I(t+1)]$.
18: $\widetilde{E}[I(t+1)] = \widetilde{E}[I(t)] + w_I(\widehat{E}[I(t+1)] - \widehat{E}[I(t)])$
19: END FOR